A note on rank-deficiency and numerical modeling

Klaus Neymeyr[a,b], Mathias Sawall[a], Tomass Andersons[a]

[a] *Universität Rostock, Institut für Mathematik, Ulmenstraße 69, 18057 Rostock, Germany*
[b] *Leibniz-Institut für Katalyse, Albert-Einstein-Straße 29a, 18059 Rostock*

Abstract

Linearly dependent concentration profiles of a chemical reaction can result in a spectral data matrix with a chemical rank smaller than the number of absorbing chemical species. Such a rank-deficiency is problematic for a factor analysis as some information on the pure component spectra cannot be recovered from the mixture data. Matrix augmentation can break rank-deficiencies and enable successful pure component recovery. In contrast to this, an artificial breakdown of a rank-deficiency can be caused by a numerical finite precision simulation of the underlying kinetic model and can fake a successful MCR analysis. This work discusses the problem and points out some remedies.

Key words: Rank-deficiency, Michaelis-Menten kinetic, MCR analysis

1. Introduction

The starting point of this note on rank-deficiency and numerical modeling was a discussion among some participants of a chemometric conference in 2022 on the Michaelis-Menten kinetics. There were different points of view on the nature of the rank-deficiency underlying the Michaelis-Menten model and on the possibility of a reconstruction of all pure component spectra from model data. We take this discussion as an impulse to investigate the interplay between rank-deficiency and the numerical modeling of rank-deficient chemical reaction systems by a computer. In this study, we focus on the Michaelis-Menten system and consider model data and experimental spectral data from rhodium-catalyzed olefin hydroformylation. We emphasize that the properties studied are of general importance for rank-deficient chemical reaction systems.

1.1. On the concepts of rank and rank-deficiency in chemometrics and mathematics

It is worth discussing the concepts of rank and rank-deficiency in chemometrics and mathematics in a comparative way.

1. *Rank of a matrix:* The (mathematical) rank of a matrix is defined as the dimension of its column space (or row space), or equivalently, the maximal number of linearly independent columns (or rows) [10]. The rank equals the number of nonzero singular values of the matrix, which result from a singular value decomposition (SVD). In linear algebra, a matrix $M \in \mathbb{R}^{m_1 \times m_2}$ is said to be *rank-deficient* if $\operatorname{rank}(M) < \min(m_1, m_2)$. These strict definitions of the rank and rank-deficiency are not used in this work because they do not tolerate even a marginal amount of noise or small rounding errors. Small perturbations are unavoidable in experimental data or in any numerical computation.
2. *Numerical rank of a matrix:* Numerical mathematics provides the notion of the numerical rank of a matrix. The numerical rank or ε-rank of a matrix is the number of its singular values that are greater than a certain small threshold parameter $\varepsilon > 0$. For example, MatLab uses $\varepsilon = \max(m_1, m_2)\operatorname{eps}(\|M\|_2)$ with $M \in \mathbb{R}^{m_1 \times m_2}$. Therein $\operatorname{eps}(z)$ is the floating-point relative accuracy, namely the distance from the absolute value of z to the next larger floating-point number, and $\operatorname{eps}(1)$ is the so-called machine precision, which equals 2.2204E-16 for double precision (64-bit) computer arithmetic. Furthermore, $\|M\|_2$ is the spectral norm of the matrix M, which is equal to its largest singular value. This choice of ε serves to ignore all singular values less than ε whose origin can be seen in the finite precision arithmetic of a computer and in the iterative nature of the SVD algorithm. This justifies the definition of the numerical rank. This notion of the numerical rank can be extended to the definition of a *numerical rank-deficiency* only by using the numerical rank of M. See [9] for more details.
3. *Chemical rank of a data set:* The issues of defining the concept of a rank are even more difficult when considering matrices with experimental (chemical) data. For example, Malinowski [16] has devoted some sections in his book "Factor Analysis in Chemistry" to the determination of the number of chemical factors and to methods of rank determination; see also [24, 25] for chemical rank determination by subspace comparison and morphological scores. Chemometric literature uses the notion of the chemical rank, which is also called a pseudo-rank

or sometimes just a rank. The noise level in experimental data is typically much larger than the level of perturbation due to rounding errors in numerical calculations. Therefore, the numerical rank is not applicable to matrices of experimental, measured data. The chemical rank of a chemical data matrix is the number of chemically relevant singular values, i.e. the number of singular values greater than a certain tolerance $\varepsilon_{\text{chem}}$. The tolerance parameter is not always easy to determine, and estimating the number of chemical species is often a problem in chemometrics.
To establish the notion of rank-deficiency for data sets in chemometrics, we consider the multivariate curve resolution (MCR) problem. To this end, we look at a spectral measurement of k spectra at n spectral channels of an ongoing chemical reaction (or other systems) and store the spectra in a $k \times n$ spectral data matrix D. According to the Lambert-Beer law, the MCR problem is to find an approximate factorization

$$D = CS^T + F \tag{1}$$

with a $k \times s$ matrix factor C which contains in its columns the concentration profiles of the s pure species. The columns of the $n \times s$ matrix factor S are the associated pure component spectra. The matrix elements of the error term matrix F are ideally equal to zero. Otherwise, they can comprise small measurement errors, deviations from bilinearity and other perturbations. In chemometrics, an experimental data matrix D is said to be *rank-deficient* if the chemical rank is less than the number s of chemical species. If a chemist or data analyst is aware of rank-deficiency in a chemical data set, then it can be resolved by matrix augmentation, standard addition and other variations of the experiment, see, e.g., [19, 7]. This work does not focus on experimental techniques to resolve the rank-deficiency, but on successfully modeling rank-deficient data sets.

4. *Nonnegative rank of a matrix:* A further definition of a rank number refers to the factorization problem (1) with $F = 0$. A nonnegative $k \times n$ matrix D has the nonnegative rank m (this is written as $\text{rank}_+(D) = m$) if m is the smallest integer such there exist nonnegative matrices $C \in \mathbb{R}^{k \times m}$ and $S \in \mathbb{R}^{n \times m}$ with m columns. The nonnegative rank of a matrix is closely related to rank-deficiency, namely when $\text{rank}(D) < \text{rank}_+(D)$, see [5] or Chap. 3 in [8]. Then more than $\text{rank}(D)$ nonnegative profiles are required to find a nonnegative factorization of D.

Next we make use of the different definitions of rank numbers and and use them to investigate the Michaelis-Menten kinetics.

1.2. The Michaelis-Menten kinetics

The Michaelis-Menten kinetics including the enzyme **E**, the substrate **S**, the enzyme-substrate complex **ES** and the product **P** reads

$$\mathbf{S} + \mathbf{E} \underset{k_2}{\overset{k_1}{\rightleftharpoons}} \mathbf{ES} \xrightarrow{k_3} \mathbf{P} + \mathbf{E}. \tag{2}$$

The associated system of nonlinear ordinary differential equations (ODE) is given by

$$\begin{aligned}
\frac{dc_{\mathbf{S}}(t)}{dt} &= -k_1 c_{\mathbf{E}}(t) c_{\mathbf{S}}(t) + k_2 c_{\mathbf{ES}}(t), \\
\frac{dc_{\mathbf{E}}(t)}{dt} &= -k_1 c_{\mathbf{E}}(t) c_{\mathbf{S}}(t) + (k_2 + k_3) c_{\mathbf{ES}}(t), \\
\frac{dc_{\mathbf{ES}}(t)}{dt} &= k_1 c_{\mathbf{E}}(t) c_{\mathbf{S}}(t) - (k_2 + k_3) c_{\mathbf{ES}}(t), \\
\frac{dc_{\mathbf{P}}(t)}{dt} &= k_3 c_{\mathbf{ES}}(t)
\end{aligned} \tag{3}$$

where $c_{\mathbf{S}}(t)$ is the concentration value of **S** at the time t and so on. The number of chemical species of the Michaelis-Menten reaction (2) equals four, but the detectable rank (or chemical rank) of D is smaller. According to Amrhein et. al. [1], see also [7], it holds that

$$\text{detectable rank} = \min(\text{number of reactions} + 1, \text{absorbing species}).$$

Pairs of a forward and backward reaction (which finally define equilibria) count as a single reaction. For the system (2) with two reactions/equilibria and four chemical species the detectable rank is 3. Hence, $\text{rank}(D) = 3$ if noise and other rank-increasing impacts of the error matrix F in (1) are absent. In Sec. 3.2 we explicitly discuss the linear dependence underlying the system (3).

However, numerical solution by a time discretization of (3) and subsequent approximate numerical integration often produces a spectral data matrix with the rank 4. Additionally, we observe that this rank-increasing numerical

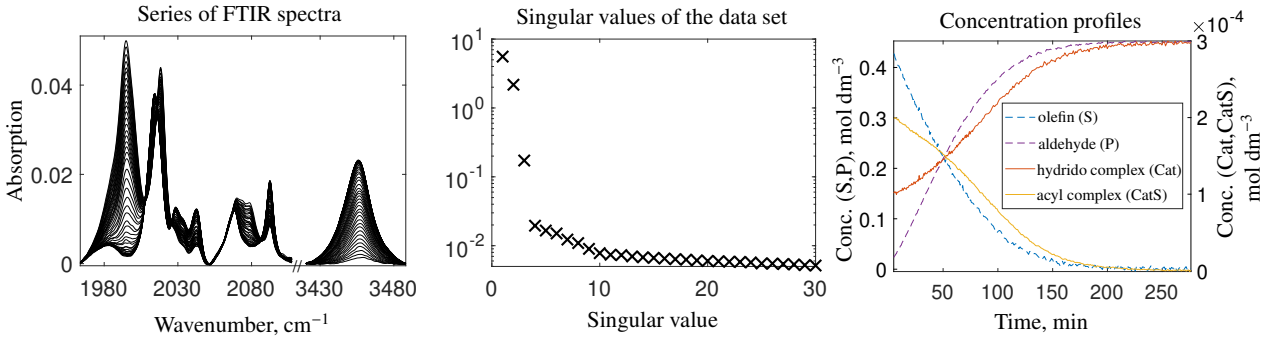

Figure 1: A rank-deficient experimental data set from the rhodium-catalyzed olefin hydroformylation process (left). The 30 largest singular values of this data set (middle) clearly indicate the rank 3 whereas four chemical species are active. The pure component analysis leads to four concentration profiles (right). The dashed concentration profiles of the olefin (S) and of the aldehyde (P) refer to the left axis. The much smaller concentration values of the catalytically active species, namely the hydrido complex (Cat) and acyl complex (CatS), correspond to the right axis.

error can sometimes be used to reconstruct missing chemical information, which is an artificial effect of the numerical simulation. This means that not only the numerical rank is 4, but the chemical rank is also 4. Poor numerical simulation is responsible for this behavior. Such a reconstruction is not possible for experimental spectral data (if (3) is assumed and, for example, there are no additional diffusion terms). This work describes and analyzes these relationships.

1.3. Rhodium-catalyzed olefin hydroformylation and the Michaelis-Menten model

In order to demonstrate that our model assumptions can be justified by experimental spectroscopic data sets, we consider the rhodium-catalyzed olefin hydroformylation with in-situ high-pressure FTIR spectroscopy, see [15, 14] for details. A certain spectral window enables an excellently resolved and isolated spectroscopic analysis of the catalyst behavior. We use a spectroscopic measurement with 300 spectra in the time interval $[4.9, 276.2]$ min at 879 wavelengths in the spectral windows $[1963.8, 2107.4] \cup [3410.9, 3478.6]$ cm^{-1}. Comparable data sets have been analysed in other publications, see, e.g., [21], where also an analysis has been presented within the U- and V-spaces which is closely related to the factor ambiguity analysis as presented in Sec. 6 of this work.

In-situ metal-organic catalysis provides many examples of reaction systems with an underlying Michaelis-Menten kinetics. Garland and coworkers [4] and other groups have presented precise spectroscopic analyses of such reaction systems. Typically, not only the substrate (an olefin species) and the product (an aldehyde) are spectroscopically observable in these measurement, but also the catalytically active species. The crucial point is that the sharp and isolated peaks of FTIR spectroscopy make it possible to observe the spectral signature of the catalyst and its precursor and that these signals are not covered by the peaks of the olefin and the aldehyde with their much higher concentration values. In detail, in-situ FTIR spectroscopy allows us to identify the acyl complex and the hydrido complex within a certain wavelengths window and to study the dynamics of these metal-organic complexes. Thus, all four chemical species of the Michaelis-Menten system (2) contribute to the measured data, but the chemical rank of the data set is only 3. This is illustrated with the help of the singular values plotted in Fig. 1. We observe a rank-deficiency in this experimental data set. Finally, the Michaelis-Menten kinetics enables a very good fit of to the chemometrically found concentration profiles [15, 14].

1.4. Organization of the paper

First, Section 2 presents the numerical discretization of the Michaelis-Menten system and discusses the impact of finite precision ODE solvers on the numerical rank of the modeled concentration factor matrix C. Section 3 shows a way how to solve the kinetic equations (3) in a way so that the finite precision of the ODE solver cannot increase the numerical rank of the concentration factor. Section 4 shows how a poor numerical solution of the Michaelis-Menten model can result in a factor C with the numerical rank 4 and how this effect can result in misinterpretations. Section 5 discusses how to add noise to the model. A geometric interpretation of such rank-deficiencies in the abstract U- and V-spaces is given in Section 6.

2. Numerical discretization and modeling

For numerical experiments with the Michaelis-Menten model (3) we use the kinetic parameters $k_1 = 20$, $k_2 = 0.1$ and $k_3 = 3$. The initial concentration values are taken as $c_{\mathbf{S}}(0) = 1$, $c_{\mathbf{E}}(0) = 0.001$ and $c_{\mathbf{ES}}(0) = c_{\mathbf{P}}(0) = 0$. The differential equation is adaptively solved with MatLab ODE solvers on the time interval $[0, 700]$ and output is

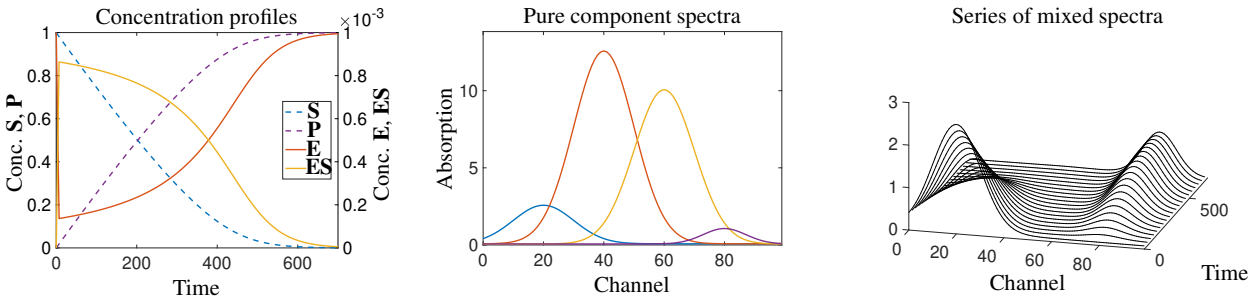

Figure 2: Concentration profiles (left) and spectra (center) for the Michaelis-Menten problem introduced in Sec.2. The color code is (**S**,**E**,**ES**,**P**)=(blue,red,ochre,purple). From the full series of mixed data the first five spectra are plotted and then only every fifth spectrum (right plot). The spectra change rapidly only in the initial phase of the reaction.

ODE solver	RelTol	AbsTol	$\sigma_4(C)$	$\max(k,s)\text{eps}(\|\|C\|\|_2)$	rank(C)	$\sigma_4(\widehat{C})$	rank($\widehat{C}$)
ode15s	1E-3	1E-6	8.2727E-13	8.8818E-14	4	1.7877-18	3
ode15s	1E-9	1E-12	1.4950E-13	8.8818E-14	4	4.1785E-18	3
ode15s	1E-11	1E-10	1.3806E-14	8.8818E-14	3	1.7201E-18	3
ode23s	1E-2	1E-5	4.77640E-13	8.8818E-14	4	2.8090E-18	3
ode23s	1E-3	1E-6	5.3463E-14	8.8818E-14	3	1.3395E-18	3
ode45	1E-3	1E-6	3.0295E-18	8.8818E-14	3	1.2.2439E-18	3

Table 1: The table shows the tolerance parameters 'RelTol' and 'AbsTol', the 4th singular value and the numerically computed rank of the concentration factor matrix C of the Michaelis-Menten system (3) for the three MatLab ODE solvers *ode15s*, *ode23s* and *ode45*. Numerically, the concentration factor matrix has the rank 4 if the numerical precision of the ODE solver is not sufficient. The last two columns refer to the matrix factor $\widehat{C}$ as computed by the stable approach explained in Sec. 3.2.

presented for 100 equidistant nodes. The pure component spectra are built from the scaled, shifted Gaussians plus offsets

$$\begin{aligned} s_1(\nu) &= \frac{5}{2}\exp\Big(-\frac{(\nu-20)^2}{200}\Big)+0.075, & s_2(\nu) &= \frac{25}{2}\exp\Big(-\frac{(\nu-40)^2}{200}\Big)+0.075, \\ s_3(\nu) &= 10\exp\Big(-\frac{(\nu-60)^2}{200}\Big)+0.065, & s_4(\nu) &= \exp\Big(-\frac{(\nu-80)^2}{100}\Big)+0.065. \end{aligned} \tag{4}$$

These functions are numerically evaluated in the interval $[0, 99]$ at $n = 100$ equidistant nodes. With $C \in \mathbb{R}^{100\times 4}$ and $S \in \mathbb{R}^{100\times 4}$ we get $D = CS^T \in \mathbb{R}^{100\times 100}$. The spectra and concentration profiles as well as the time-series of the mixture spectra that form the rows of D are shown in Fig. 2.

Due to the linear dependence of the concentration profiles, the rank of the matrix factor C is equal to 3; see Section 3.2 for a justification. Together with $\text{rank}(S) = 4$ we get that $\text{rank}(D) = 3$. Thus, D is a rank-deficient matrix. If no pair of nonnegative 3-column matrices C and S exists with $D = CS^T$, then the nonnegative rank equals $\text{rank}_+(D) = 4$, cf. Sec. 1.1. However, numerical inaccuracies of the ODE solver (caused by the so-called discretization error) and rounding errors can in some cases result in a numerical evaluation of the rank of D to be equal to 4.

Next, we study the dependence of the fourth numerically computed singular value for the numerically solved Michaelis-Menten model. The computations are executed for varying error tolerance parameters controlling the accuracy of some prominent MatLab ODE solvers. For these computations we apply the ODE solvers *ode15s*, *ode23s* and *ode45* of MatLab. The stiff ODE solvers *ode15s* and *ode23s* use adaptive step-length variable-order strategies in combination with numerical differentiation formulas. The routine ode45 is based on an explicit Runge-Kutta formula, namely the Dormand-Prince pair, which combines a 4th order Runge-Kutta scheme with a 5th order error estimation. The routines work with the scalar relative error tolerance 'RelTol' (default value 1E-3) and the absolute error tolerance 'AbsTol' (default value for all components 1E-6) for error control. Table 1 shows the results for solving the ODE (2) for the parameter settings and initial concentrations given in the first paragraph of this section. The small concentrations of **ES** and **E** show rapid relative changes in the initial phase of the reaction. Therefore, numerical solvers for stiff ODEs seem to be very appropriate. The tolerance parameters must be set smaller than the default choice in order to reproduce numerically the correct rank 3. For the Runge-Kutta solver ode45 the default parameters are sufficient to get the correct order due to the high fifth order error estimation. Next, we discuss how to enforce a correct numerical rank determination and how a rank-4 factor C can fake a successful and complete MCR analysis.

3. How to enforce a low-rank solution

3.1. Structure-preserving numerical solvers

Discrete *numerical* solutions of ordinary (ODE) or partial (PDE) differential equations do not necessarily exhibit the properties which hold for their exact solution functions. This is a well-known phenomenon in numerical mathematics. For instance, Hamiltonian systems define ODEs for which numerical solvers often yield solutions violating the preservation of energy and angular momentum. However, so-called symplectic solvers can preserve these conservation laws [11]. Another example are the Navier-Stokes on the flow of incompressible fluids whose discrete solutions (by finite differences) show more diffusion than the original partial differential equations. Most often the additional so-called numerical diffusion should be as small as possible.

In a similar way, numerical ODE solvers for rank-deficient systems tend to increase the numerical rank of the matrix factor C as small errors break the linear dependence of some columns of C. However, one can sometimes construct algorithms which enforce and preserve the correct rank. For rank-deficient problems the kinetic ODE systems include redundant equations so that some of the right-hand sides of these systems can be expressed as linear combinations of others. For the theoretical background of such linear dependencies for rank-deficient systems see [2]. The work [6] presents an approach for finding a smallest-dimensional representation of a system of kinetic equations by using the so-called *extent of a reaction* or *degree of advancement* and also discusses limitations of these techniques.

3.2. Two key equations of the Michaelis-Menten system

Two independent mass balance equations can be formulated for the substrate species and for the enzyme/catalyst of the Michaelis-Menten system (3)

$$\frac{dc_{\mathbf{S}}(t)}{dt} + \frac{dc_{\mathbf{ES}}(t)}{dt} + \frac{dc_{\mathbf{P}}(t)}{dt} = 0 \quad \text{and} \quad \frac{dc_{\mathbf{E}}(t)}{dt} + \frac{dc_{\mathbf{ES}}(t)}{dt} = 0. \tag{5}$$

Other linear relations can also be stated, but all of them can be traced back to (5). Time integration of (5) yields the two affine dependencies

$$c_{\mathbf{S}}(t) + c_{\mathbf{ES}}(t) + c_{\mathbf{P}}(t) = \omega_1 \quad \text{and} \quad c_{\mathbf{E}}(t) + c_{\mathbf{ES}}(t) = \omega_2$$

with constants ω_1 and ω_2. (These two equations can be used for a mean centered representation [17].) These constants are determined by the initial concentration values at $t = 0$, namely $\omega_1 = c_{\mathbf{S}}(0) + c_{\mathbf{ES}}(0) + c_{\mathbf{P}}(0)$ and $\omega_2 = c_{\mathbf{E}}(0) + c_{\mathbf{ES}}(0)$. This makes it possible to eliminate two equations from (3) since the equations

$$\begin{aligned} c_{\mathbf{ES}}(t) &= c_{\mathbf{E}}(0) + c_{\mathbf{ES}}(0) - c_{\mathbf{E}}(t) \\ c_{\mathbf{P}}(t) &= c_{\mathbf{S}}(0) + c_{\mathbf{P}}(0) - c_{\mathbf{E}}(0) - c_{\mathbf{S}}(t) + c_{\mathbf{E}}(t) \end{aligned} \tag{6}$$

serve to represent $c_{\mathbf{ES}}(t)$ and $c_{\mathbf{P}}(t)$ if $c_{\mathbf{S}}(t)$ and $c_{\mathbf{E}}(t)$ are known. The reduced Michaelis-Menten system reads

$$\begin{aligned} \frac{dc_{\mathbf{S}}(t)}{dt} &= -k_1 c_{\mathbf{E}}(t) c_{\mathbf{S}}(t) + k_2 (c_{\mathbf{E}}(0) + c_{\mathbf{ES}}(0) - c_{\mathbf{E}}(t)), \\ \frac{dc_{\mathbf{E}}(t)}{dt} &= -k_1 c_{\mathbf{E}}(t) c_{\mathbf{S}}(t) + (k_2 + k_3)(c_{\mathbf{E}}(0) + c_{\mathbf{ES}}(0) - c_{\mathbf{E}}(t)). \end{aligned} \tag{7}$$

Hence, an ODE solver is only required to determine the concentration profiles of **S** and **E** by solving the two-dimensional ODE (7). The two remaining concentrations of **ES** and **P** can be evaluated by (6). With this modification a low accuracy of the numerical ODE solver cannot lead to a false rank of the concentration factor. To this end, we form the row vector of concentration functions

$$\widehat{C}(t) = [c_{\mathbf{S}}(t),\ c_{\mathbf{E}}(t),\ c_{\mathbf{E}}(0) + c_{\mathbf{ES}}(0) - c_{\mathbf{E}}(t),\ c_{\mathbf{S}}(0) + c_{\mathbf{P}}(0) - c_{\mathbf{E}}(0) - c_{\mathbf{S}}(t) + c_{\mathbf{E}}(t)]. \tag{8}$$

These functions span only a three-dimensional space. This is easy to verify because

$$\widehat{C}(t)\left(0,1,1,0\right)^T = c_{\mathbf{E}}(0) + c_{\mathbf{ES}}(0) = \omega_2 \quad \text{and} \quad \widehat{C}(t)\left(1,-1,0,1\right)^T = c_{\mathbf{S}}(0) + c_{\mathbf{P}}(0) - c_{\mathbf{E}}(0) = \omega_1 - \omega_2.$$

If $\omega_2 = 0$ or $\omega_1 - \omega_2 = 0$, then a nonzero vector z has been determined with $\widehat{C}z = 0$. If ω_2 and $\omega_1 - \omega_2$ are nonzero, then

$$z = \left(1,-1,0,1\right)^T/(\omega_1 - \omega_2) - \left(0,1,1,0\right)^T/\omega_2 \neq 0$$

and $\widehat{C}(t)z = 0$. This shows the linear dependence of the functions in $\widehat{C}(t)$. A time discretization of $\widehat{C}(t)$ with respect to a k time steps $t_1 < t_2 < \cdots < t_k$ leads us to the $k \times 4$ matrix $\widehat{C}$. A numerical SVD of $\widehat{C}$ (or $D = \widehat{C}S^T$) based on (7) and (8) and with $k = 100$ and equidistant nodes results in a fourth singular value of $\widehat{C}$ (or D) around 1E-18 (even smaller

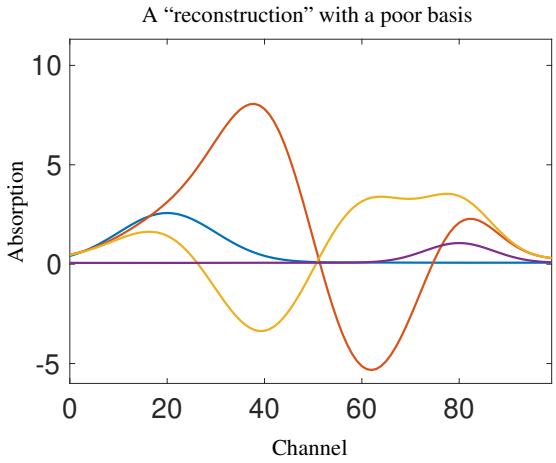

Figure 3: A least squares approximation of the *four* true spectral profiles (4) with respect to the three-dimensional basis of the three singular vectors corresponding to the spectral data matrix D with C computed according to (7) and (8). These “spectra” contain major negative entries and are very different from the true spectra shown in Fig. 2. The solution is not feasible. This confirms that the rank-deficiency is correctly treated.

than the machine precision) and a numerical rank of $\widehat{C}$ equal to 3. Table 1 shows in its last two columns the results. In order to test to what extent the basis of the three right singular vectors (the columns of V of the truncated singular value decomposition of D) is suitable for an expansion of the true four spectral profiles (4) we execute target testing based on the following MatLab commands (solution of a least-squares problem)

$$\text{coeffs = V\S;} \qquad \text{plot(V*coeffs);} \qquad \text{residual=norm(V*coeffs-S)} \tag{9}$$

and get a residual equal to 50.928 and the four spectral profiles shown in Fig. 3. These profiles have major negative parts and are very different from the true spectra shown in Fig. 2; this means that S is not in the data space of the columns of D. This confirms that the rank-deficiency is not resolvable.

4. How a lack of accuracy in numerical modeling can lead to artificial spectral recovery

The last section has shown that the pure component factors of a rank-deficient problem cannot be resolved if the kinetic equations are solved in a careful way by means of a reduced set of ODEs. This is a correct and expected result. Next, we show how an inadequate numerical solution approach can lead to an artificially successful pure component recovery as a consequence of a finite precision solution of the model equations. This is an unwanted numerical side-effect that cannot be reproduced for experimental spectral data.

To this end, we discuss again the numerical solutions of (3) by the MatLab solver *ode15s* which typically results in a concentration factor matrix C of the numerical rank 4; smaller tolerance parameters are required to achieve a concentration factor of the numerical rank 3, see Table 1. For instance, with the MatLab default values RelTol=1E-3 and AbsTol=1E-6 we first compute the matrix C with the numerical rank 4 and then the truncated SVD $D = U\Sigma V^T$ of the rank-4 matrix $D = CS^T$. Then the four column vectors of V span a space which is capable of a good recovery of all spectral profiles. In order to show this, we re-use the MatLab commands (9) and get the small reconstruction residual 1.4958E-3. The pure component spectra are almost representable from the right singular vectors and they are nearly identical to the original spectra shown in Fig. 2 (right plot). This is a surprising result as the rank-deficiency seems to have no impact - the predicted loss of information does not occur. Thus, the chemical rank was also incorrectly modeled for this the matrix.

This phenomenon is analyzed next by decreasing the error tolerance parameters of the ODE solver and simultaneously monitoring the numerical rank of D as well as the reconstruction residual. The stiff ODE solver *ode15s* is used to solve (3) with RelTol in the interval [1E-9, 1E-12] and simultaneous parameter setting AbsTol = RelTol/1000. The left plot in Fig. 4 shows the fourth singular value $\sigma_4(D)$ of $D = CS^T$. Only for the smallest RelTol settings does the numerical rank of D equal 3 and this region is plotted in red. Blue color indicates that D has the numerical rank 4. The right plot in Fig. 4 shows the associated reconstruction error of the spectral profiles according to the MatLab commands (9). Where the residual is small (D has the numerical rank 4) the four true spectral profiles are recoverable from the right singular vectors of D. The largest error is observed if D has the numerical rank 3 (red color). Only this region represents the true behavior of a rank-deficient system where the expected loss of information is observed.

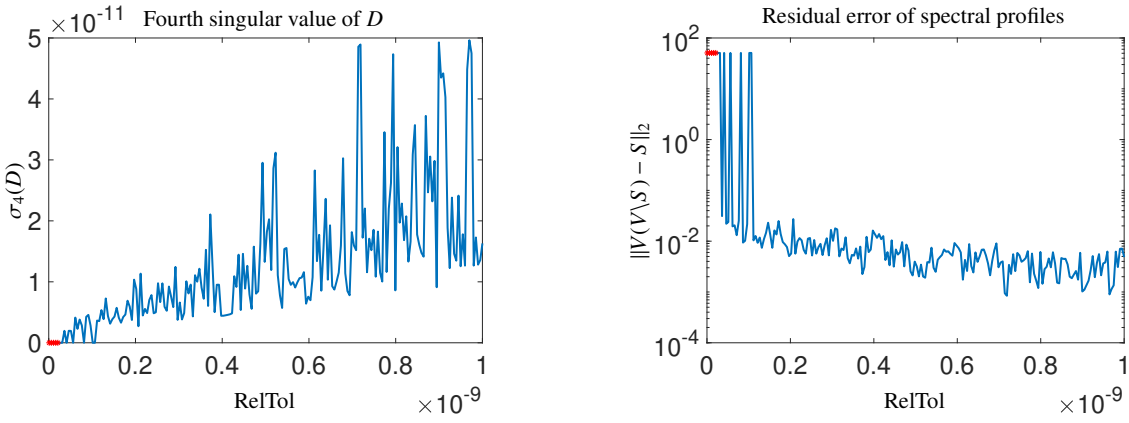

Figure 4: Numerical solution of the Michaelis-Menten kinetic equations (3) with the stiff ODE solver *ode15s* for varying tolerance parameters RelTol in the interval [1E-9, 1E-12] and simultaneous parameter setting AbsTol = RelTol/1000. The left plot shows the fourth singular value $\sigma_4(D)$. A noise-free system is considered. The non-smooth curve pattern can be traced back to numerical discretization errors. Only for the smallest RelTol settings the numerical rank of D equals 3; this region is plotted in red, whereas blue color marks that D has the numerical rank 4. The right plot shows the reconstruction error of the spectral profiles. The largest error is observed if D has the numerical rank 3 which is again marked by red color. Only for this largest residual the correct loss of information which is inherent to a rank-deficient system is observed.

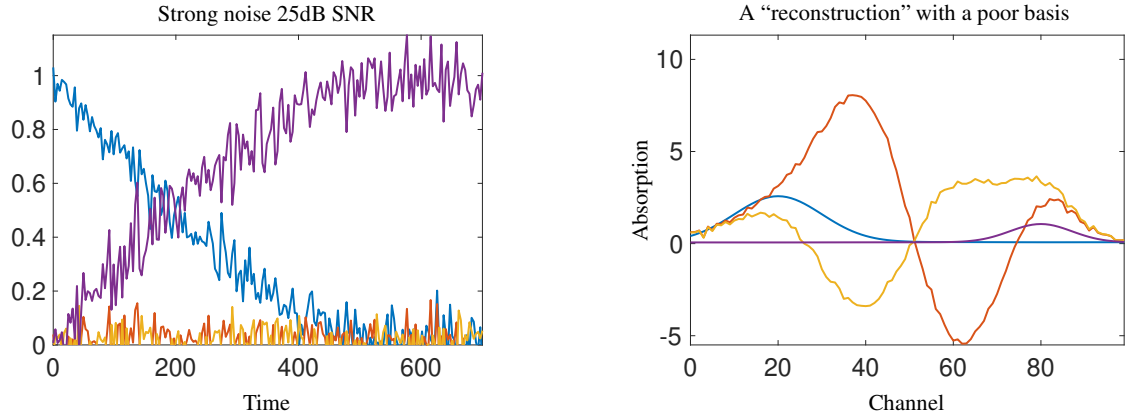

Figure 5: White Gaussian noise of any amplitude can be added to the two profiles (7) without changing the numerical rank of the concentration factor if it is constructed according to (8). The left plot shows the concentration profiles for an SNR of 25dB. Due to the correctly reproduced rank-deficiency, the rank-4 factor of the true spectral profiles cannot be recovered. The expansion of the true spectral profiles with respect to the basis of the four right singular vectors being associated with the four largest singular values results in the profiles shown in the right plot. These profiles (aside from noise) reproduce those shown in Fig. 3. This demonstrates the operability of the approach.

5. How to add noise to the concentration profiles without breaking the rank-deficiency

The analysis presented so far indicates how to add noise to the model data without destroying the rank-deficiency in the sense of chemical rank. Now, we discuss this point in detail. First, we demonstrate an inappropriate approach and add white Gaussian noise to all columns of C by using the MatLab function *awgn*$(C, 200)$ where C has been determined from solving (3) with MatLab routine *ode15s* with high precision RelTol=1E-10 and AbsTol=1E-13. Adding noise to the columns of C simulates the effects of an imprecise ODE solver, while experimental noise is simulated by adding Gaussian noise to the matrix elements of the measured data matrix D. As indicated by Table 1 this guarantees a concentration factor C with the numerical rank 3. Section 4 predicts that the true spectral profiles are not recoverable from the three right singular vectors of D. The signal-to-noise ratio (SNR) of the noise is 200dB. (For this very low noise level, a plot of the profiles looks like those in Fig. 2.) After noise addition the numerical rank of the product matrix $D = CS^T$ equals 4 (which is not very surprising) and its fourth singular value equals 6.6785E-8. Re-running the commands (9) yields a residual of the value 1.0711E-6. This shows that the true spectral profiles are very well reconstructable from the right singular vectors of D. Therefore, this is a biased type of noise addition, which artificially allows the rank-deficiency to be broken and to reconstruct the true spectral profiles from the additional information contained in the noisy data.

How can noise be added to C without breaking the rank-deficiency of D? The straightforward approach is to compute the two profiles of the species **S** and **E** according to (7). Any, even-low accuracy ODE solver can be used. Regardless of the numerical precision of the solver, the numerical rank of the resulting two-column matrix necessarily

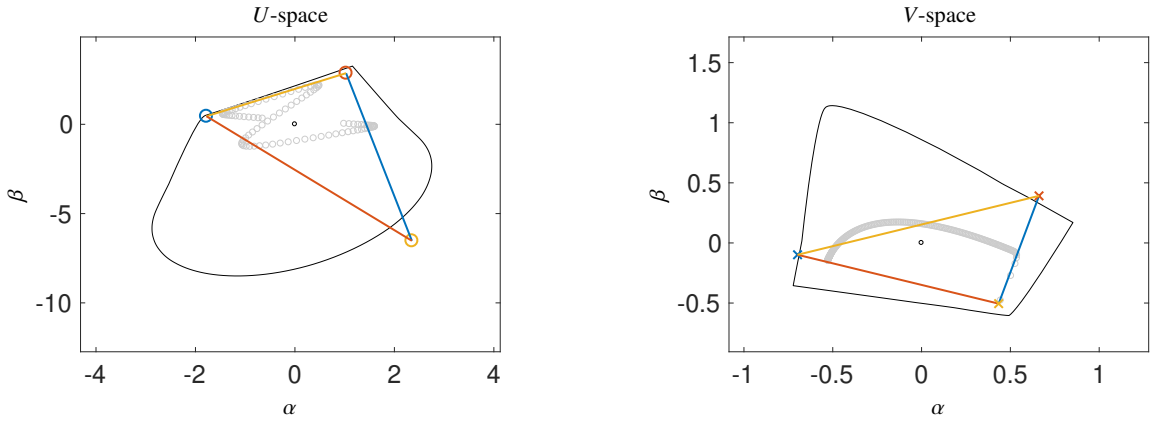

Figure 6: For the spectral data matrix D generated with $c_{\mathbf{E}}(0) = 0.1$ and *ode15s* with RelTol=1E-3 and AbsTol=1E-6 the numerical rank of D is 4. Exploring the geometry in the two-dimensional U- and V-spaces (spanned only by the respective three dominant singular vectors) by means of the FACPACK module 'Duality & AFS' no pair of triangles can be constructed which each enclose the data representing points (marked by gray circles) and which are simultaneously contained in the outer polygon (marked by solid black curves). The plotted colored triangles are not feasible. The non-constructabililty of a nonnegative pair of factors C and S indicates that rank-3 factors cannot solve the factorization problem for D. This is consistent with the rank-deficiency.

equals 2. Then the concentration factor C is formed according to (8). By construction, this factor has the numerical rank 3. Figure 5 (left) shows the concentration profiles with the low SNR ratio of 25dB. (We note the proposed operation of noise addition to C has no practical importance for simulating noise addition to the data set D. Our intention is to demonstrate that the reduced two-species subsystem can be altered in any way, e.g., with noise, without changing the rank of the four-species factor C.) Due to the correctly reproduced rank-deficiency, the rank-4 factor of the true spectral profiles cannot be recovered. The expansion of the true spectral profiles with respect to the basis of the four dominant right singular vectors is shown in the right plot of Fig. 5. These profiles (aside from noise) reproduce those shown in Fig. 3. The true profiles cannot be recovered. This demonstrates the operability of the approach. Noise addition is not restricted to the concentration factor and is also possible for the spectral factor S. Noise addition to the $n \times 4$ matrix S cannot increase its numerical rank that is always bounded by its second dimension 4. Usually, noise is directly added to the spectral data matrix D. If a precise rank-3 factor C is used to form $D = CS^T$ as a rank-deficient rank-3 matrix, then noise addition to D will increase its numerical rank. However, this non-biased noise cannot be used in order to recover the four true spectral profiles.

6. Geometric analysis in the U- and V-space

Rank-deficiency can also be well-understood by a geometric representation in the abstract U- and V-space [3, 22], which are spanned by the bases of left and right singular vectors of D. The letters U and V refer to the SVD $D = U\Sigma V^T$. The columns of U contain the left singular vectors and the columns of V the right singular vectors. The singular values form the diagonal of the diagonal matrix Σ.

Next, we consider the spectral data D generated by *ode15s* with RelTol=1E-3 and AbsTol=1E-6. The low accuracy results in the increased numerical rank 4 of D, cf. Table 1. We observe that for this data set the third and the fourth singular values are very small, namely $\sigma_3 = 0.0875$ and σ_4 =4.2145E-11. This results in a qualitatively different behavior in the U- and V-space than that of the experimental rhodium catalyzed hydroformylation process, see Sec. 1.3. To mimic the experimental finding in our model, we have increased the absorptivities of **E** and **ES** by a factor of 100. After this change, the observations on the behavior of the ODE solver made in the previous sections are still valid. Then we get $\sigma_3 = 11.954$ and σ_4 =9.4156E-8. Because of the large ratio σ_3/σ_4 >1E8, we first consider a truncated SVD based on only $s = 3$ singular vectors so that the associated abstract U- and V-spaces are $(s-1=2)$-dimensional. In these spaces the convex hull of the vectors

$$a_i := \frac{((U\Sigma)(i, 2:s))^T}{(U\Sigma)(i, 1)} \tag{10}$$

for $i = 1, \ldots, k$ is the inner polygon in the V-space for a $k \times n$ matrix D. The convex hull of

$$b_j := \frac{V^T(2:s, j)}{V^T(1, j)} \tag{11}$$

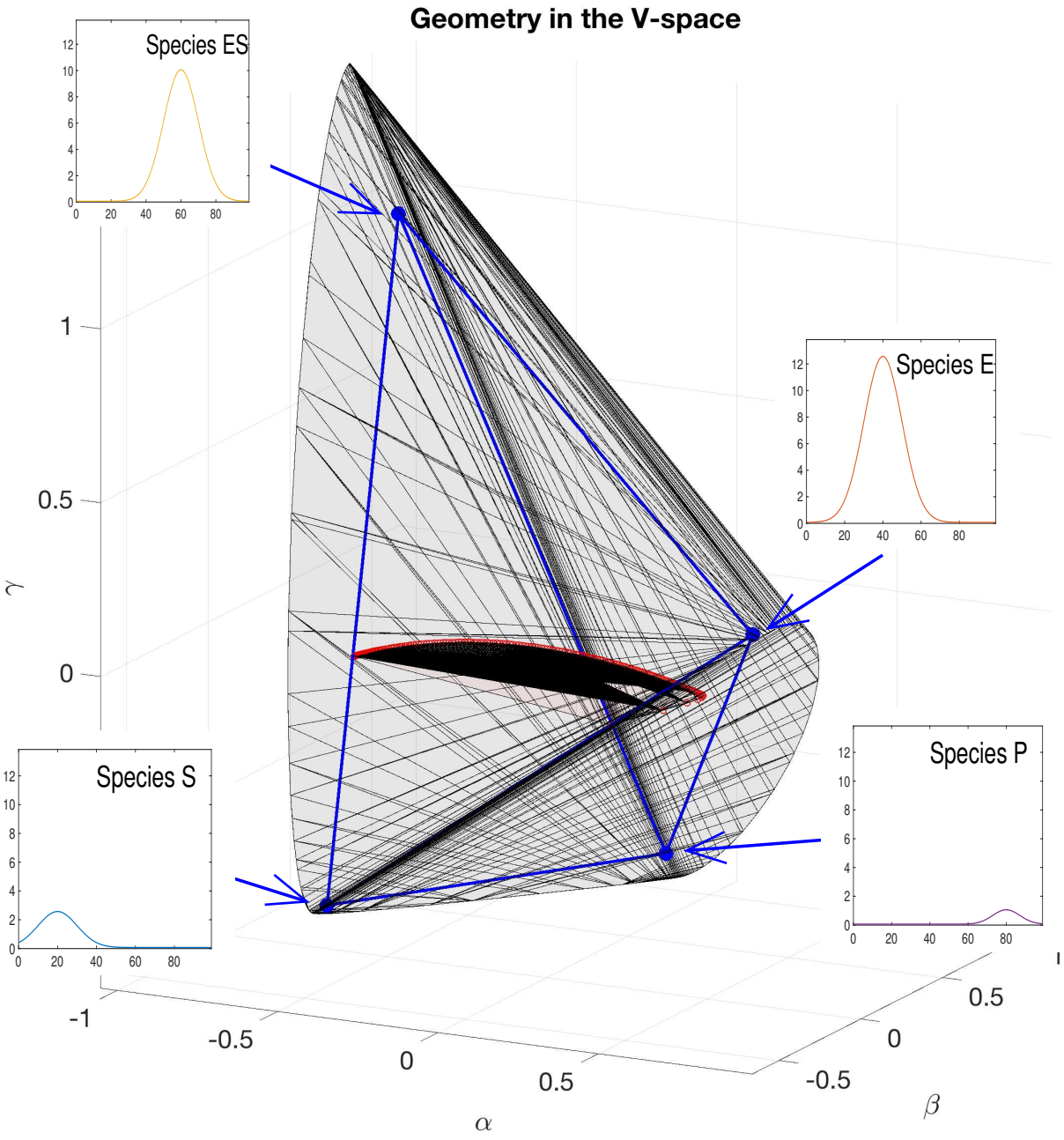

Figure 7: In the three-dimensional V-space a feasible solution can be constructed, see Sec. 6 for details on the data set, namely D is generated by *ode15s* with RelTol=1E-3 and AbsTol=1E-6. The two-dimensional V-space as shown in Fig. 6 (right plot) is embedded in the 2D plane $(\alpha, \beta, 0)$. The data representing vectors are plotted by red stars and the almost planar inner polyhedron is shown in light red. The outer polyhedron is the large gray set which encloses the blue tetrahedron. The four vertices of this tetrahedron represent the true spectra, namely the columns of the matrix factor S as also shown in Fig. 2.

for $j = 1, \ldots, n$ is the inner polygon in the U-space. Figure 6 shows these data representing vectors a_i and b_j by gray circles in the respective abstract spaces. The associated outer polygons are plotted by bold black lines and represent the nonnegativity constraints. A feasible nonnegative factorization of D with three-column factors C and S^T would correspond to a pair of triangles which enclose the respective inner polygon each and which are enclosed in the respective outer polygon. The FACPACK software [21] (we have used the Duality & AFS module) allows to try out such triangle constructions. The two triangle constructions are not independent, but entangled by so-called duality relations [12, 18, 20]. The results of such a non-successful triangle construction are shown in Fig. 6. In both cases a single vertex of a triangle has left the outer polygon and also an edge intersects the interior of the inner polygon. No feasible triangles can be constructed. This is a clear indicator for a rank-deficiency of the data matrix D. The existence of a feasible quadrangle implies that the nonnegative rank is 4.

In a second step we consider the same construction, but now with a fourth singular vector. The vectors (10) and (11) are computed for $s = 4$. Fig. 7 shows the V-space representation in three dimensions. This plot embeds the two-dimensional V-space as shown in Fig. 6 (right plot) in the 2D plane $(\alpha, \beta, 0)$ through the origin, cf. [23]. Here the data representing vectors (10) are plotted by red stars and the almost planar inner polyhedron in shown in light red. Its volume in three dimensions is small, namely 8.1419E-10. In contrast to this, the approximate two-dimensional volume (area) in the V-space is about 0.42031. The reader can roughly check this by estimating the area of the inner polygon in the right plot of Fig. 6.

These findings suggest that the fourth singular value should not make a significant contribution to the system, and this problem should be regarded to be of rank-3 with rank-deficiency. Here, however, the spectral data appears as a rank-4 problem with no rank-deficiency due to the inappropriate numerical modelling. Moreover, the further dimension helps to find a nonnegative factorization. These geometric relations are demonstrated in Fig. 7 where the outer polyhedron is the large gray set enclosing a blue tetrahedron which again encloses the inner polyhedron. The four vertices of the blue tetrahedron represent the true spectral profiles, namely the columns of the matrix factor S. Together with the associated construction in the U-space, where also a dual tetrahedron with the corresponding properties can be constructed, this proves that this case presents itself as a rank-4 problem with no rank-deficiency, despite the reaction kinetics. In a correctly modelled system, the fourth singular value should contain no additional information that enables the reconstruction of the original factorization.

Geometrically, this unsuitable modeling approach of a four-component rank-deficient system is characterized by an almost flat inner polyhedron for which tetrahedron constructions are possible and for which the corresponding triangle constructions in the planes $(\alpha, \beta, 0)$ in the U- and V-spaces are not possible. The considered geometric construction approach is stable in a sense that numerical errors which have made D to a rank-4 matrix do not harm the construction. These relationships also hold true for higher dimensions, ergo for systems with a larger number of chemical species.

7. Conclusion

The first letters of each sentence on the preface of the classic textbook *Analysis of Numerical Methods* by Isaacson and Keller [13], when put together, make up the sentence "Down With Computers And Their Lackeys". This is a critical, well-hidden and surprising message for a book on numerical methods. Is this judgement on computers in general too harsh? After all, computers have played such a central role in sciences, including chemometrics. However, computational results should always be viewed critically and accompanied by numerical analysis.

We have shown that discretization errors of numerical ODE solvers are a pitfall for the numerical modeling of rank-deficient systems (here for the Michaelis-Menten system). The rank-deficiency can be destroyed and the resulting inaccurate model data can show very different behavior to that observed with experimentally obtained spectral data. However, by increasing the numerical accuracy or reducing the dimension of the ODE, the rank-deficiency can be reproduced numerically to such an extent that numerical modeling of such systems remains a valuable tool for chemometric analysis. Furthermore, our analysis is closely related to the question how to add noise to a model without breaking the rank-deficiency.

Acknowledgements

The authors would like to express their gratitude to Dr. Christoph Kubis (Leibniz Institute for Catalysis in Rostock, Germany) for providing the experimental data set from Section 1.3.

References

[1] M. Amrhein, B. Srinivasan, D. Bonvin, and M. M. Schumacher. On the rank deficiency and rank augmentation of the spectral measurement matrix. *Chemom. Intell. Lab. Syst.*, 33(1):17–33, 1996.

[2] J. Billeter, Y.-M. Neuhold, and K. Hungerbühler. Systematic prediction of linear dependencies in the concentration profiles and implications on the kinetic hard-modelling of spectroscopic data. *Chemom. Intell. Lab. Syst.*, 95(2):170–187, 2009.
[3] O.S. Borgen and B.R. Kowalski. An extension of the multivariate component-resolution method to three components. *Anal. Chim. Acta*, 174:1–26, 1985.
[4] W. Chew, E. Widjaja, and M. Garland. Band-target entropy minimization (BTEM): An advanced method for recovering unknown pure component spectra. Application to the FT-IR spectra of unstable organometallic mixtures. *Organometallics*, 21(9):1982–1990, 2002.
[5] J. E. Cohen and U. G. Rothblum. Nonnegative ranks, decompositions, and factorizations of nonnegative matrices. *Linear Algebra Appl.*, 190:149–168, 1993.
[6] A.E. Croce. The application of the concept of extent of reaction. *J. Chem. Educ.*, 79(4):506, 2002.
[7] A. de Juan, S. Navea, J. Diewok, and R. Tauler. Local rank exploratory analysis of evolving rank-deficient systems. *Chemom. Intell. Lab. Syst.*, 70(1):11–21, 2004.
[8] N. Gillis. *Nonnegative matrix factorization*. Society of Industrial and Applied Mathematics, Philadelphia, 2021.
[9] G. Golub, V. Klema, and G.W. Stewart. *Rank degeneracy and least squares problems*. Stanford University, California, Department of Computer Science, 1976.
[10] G.H. Golub and C.F. Van Loan. *Matrix Computations*. Johns Hopkins Studies in the Mathematical Sciences. Johns Hopkins University Press, Baltimore, MD, 2013.
[11] E. Hairer, C. Lubich, and G. Wanner. *Geometric numerical integration*. Springer, 2002.
[12] R.C. Henry. Duality in multivariate receptor models. *Chemom. Intell. Lab. Syst.*, 77(1-2):59–63, 2005.
[13] E. Isaacson and H.B. Keller. *Analysis of Numerical Methods*. Wiley, New York, 1966.
[14] C. Kubis, M. Sawall, A. Block, K. Neymeyr, R. Ludwig, A. Börner, and D. Selent. An operando FTIR spectroscopic and kinetic study of carbon monoxide pressure influence on rhodium-catalyzed olefin hydroformylation. *Chem.-Eur. J.*, 20(37):11921–11931, 2014.
[15] C. Kubis, D. Selent, M. Sawall, R. Ludwig, K. Neymeyr, W. Baumann, R. Franke, and A. Börner. Exploring between the extremes: Conversion dependent kinetics of phosphite-modified hydroformylation catalysis. *Chem. Eur. J.*, 18(28):8780–8794, 2012.
[16] E. Malinowski. *Factor analysis in chemistry*. Wiley, New York, 2002.
[17] R.J. Pell, M.B. Seasholtz, and B.R. Kowalski. The relationship of closure, mean centering and matrix rank interpretation. *J. Chemom.*, 6(1):57–62, 1992.
[18] R. Rajkó. Natural duality in minimal constrained self modeling curve resolution. *J. Chemom.*, 20(3-4):164–169, 2006.
[19] J. Saurina, S. Hernández-Cassou, R. Tauler, and A. Izquierdo-Ridorsa. Multivariate resolution of rank-deficient spectrophotometric data from first-order kinetic decomposition reactions. *J. Chemom.*, 12(3):183–203, 1998.
[20] M. Sawall, A. Jürß, H. Schröder, and K. Neymeyr. Simultaneous construction of dual Borgen plots. I: The case of noise-free data. *J. Chemom.*, 31:e2954, 2017.
[21] M. Sawall, C. Kubis, D. Selent, A. Börner, and K. Neymeyr. A fast polygon inflation algorithm to compute the area of feasible solutions for three-component systems. I: Concepts and applications. *J. Chemom.*, 27:106–116, 2013.
[22] M. Sawall and K. Neymeyr. On the area of feasible solutions for rank-deficient problems: I. Introduction of a generalized concept. *J. Chemom.*, 35(3):e3316, 2020. e3316 cem.3316.
[23] M. Sawall, C. Ruckebusch, M. Beese, R. Francke, A. Prudlik, and K. Neymeyr. An active constraint approach to identify essential spectral information in noisy data. *Anal. Chim. Acta*, 1233:340448, 2022.
[24] H. Shen, Y. Liang, O.M. Kvalheim, and R. Manne. Determination of chemical rank of two-way data from mixtures using subspace comparisons. *Chemom. Intell. Lab. Syst.*, 51(1):49–59, 2000.
[25] H. Shen, L. Stordrange, R. Manne, O.M. Kvalheim, and Yizeng Liang. The morphological score and its application to chemical rank determination. *Chemom. Intell. Lab. Syst.*, 51(1):37–47, 2000.